Simplified Model Analysis of Wave Interaction with Flexible Piezoelectric Film Structures (Post-print)

Authors: Wenyu Yang

Date: 2025-11-01T00:00:00+00:00

Abstract

Piezoelectric materials can be utilized to capture ocean wave energy, converting wave energy directly into electrical energy. The combination of piezoelectric membranes with flexible membranes to constitute a submerged breakwater structure can serve as a novel wave energy conversion device with the dual functions of wave power generation and wave attenuation. This study derives the dimensionless motion equation for flexible piezoelectric membrane structures and investigates the interaction between waves and flexible piezoelectric membrane structures through numerical wave flume simulations based on potential flow theory. A prediction method for the added mass of flexible piezoelectric membrane structures is presented, and the primary control parameters influencing the motion response of flexible piezoelectric membrane structures are discussed. The motion response of flexible piezoelectric membrane structures under wave action satisfies a nonlinear vibration differential equation, wherein the nonlinear term is controlled by the dimensionless membrane structural elastic modulus E. *The resonance period of flexible piezoelectric membrane structures is obtained, and a computational fitting formula for the dimensionless added mass of flexible piezoelectric membrane structures is provided; when the dimensionless initial tension T*0 ranges from 1.31 × 10^-5 to 6.33 × 10^-4, the range of the critical control parameter E* for linear and nonlinear responses of flexible piezoelectric membranes is given.

Full Text

Simplified Analysis of Interactions Between Water Waves and Flexible Piezoelectric Membrane Structures

YANG Wenyu, LIU Chunrong
(School of Civil Engineering and Architecture, Xiamen University of Technology,

Xiamen 361024, China)

Abstract: Piezoelectric materials can be used to capture ocean wave energy, converting it directly into electrical energy. Combining piezoelectric membranes with flexible membranes to form a submerged breakwater structure can serve as a novel wave energy conversion device with dual functions of power generation and wave attenuation. This study derives the dimensionless motion equations for flexible piezoelectric membrane structures and investigates wave-structure interactions using a numerical wave flume based on potential flow theory. A prediction method for the added mass of flexible piezoelectric membranes is presented, and the main control parameters affecting the dynamic response of the structure are discussed. The motion response of flexible piezoelectric membranes under wave action satisfies a nonlinear vibration differential equation, with the nonlinear term controlled by the dimensionless membrane elastic modulus E^*. The resonant period of the flexible piezoelectric membrane is obtained, and a fitted formula for calculating its dimensionless added mass is provided. When the dimensionless initial tension T_0^* ranges from 1.31×10^{-5} to 6.33×10^{-4}, the critical control parameter range for E^* governing linear and nonlinear responses is identified.

Keywords: flexible piezoelectric membrane; resonance period; added mass; wave energy dissipation; wave energy

1. Introduction

Ocean wave energy, as a clean energy source, offers an effective alternative to fossil fuels. Common wave energy conversion principles involve capturing wave energy and transforming it into mechanical energy, which is then converted into electricity [1-2]. Piezoelectric materials, a new class of materials developed in recent years, can directly convert ocean wave energy into electrical energy [3]. BURNS [4] first combined piezoelectric materials with wave energy development, designing a piezoelectric wave power generation device. Subsequently, researchers have proposed various structural configurations for piezoelectric wave energy converters, most commonly cantilever beam structures with piezoelectric patches or oscillating systems coupled with piezoelectric materials installed near the free surface of seawater [5-9]. Notably, NABAVI et al. [8] conducted field tests on piezoelectric conversion devices installed on buoy structures in Boston Bay and San Francisco Bay, achieving output power densities of 8.57 kW/m^3 and 11.4 kW/m^3, respectively, demonstrating promising prospects for piezoelectric wave energy generation.

Combining piezoelectric membranes with flexible membranes to form a sealed flexible piezoelectric membrane structure installed on the seabed can function as both a novel wave energy conversion device and a submerged breakwater, offering dual capabilities of power generation and wave attenuation [10]. Therefore, the dynamic response of flexible piezoelectric membranes under wave action

plays a crucial role in their energy conversion and wave dissipation functions. Scholars have conducted theoretical, experimental, and numerical studies on flexible membrane breakwaters. OHYAMA et al. [11] experimentally investigated the wave transmission and reflection coefficients of bottom-seated water-filled flexible membrane breakwaters. PHADKE et al. [12-14] used boundary element and finite element methods to study the resonant and nonlinear responses of bottom-seated water-filled flexible membranes under wave action. STAMOS et al. [15] experimentally compared the wave attenuation performance of rigid and flexible bottom-seated breakwaters, finding that semi-cylindrical flexible bottom-seated breakwaters exhibited better wave reflection. DAS et al. [16] developed a coupled boundary element and finite element model for three-dimensional flexible membrane breakwaters. LIU et al. [17] simulated the nonlinear interaction between flexible membrane breakwaters and waves using an Euler-Lagrange method. ZHAO et al. [18] investigated the wave dissipation mechanism of flexible water bag submerged breakwaters through numerical simulation and experiments. LI et al. [19] analyzed the hydroelastic interaction between waves and semi-circular flexible membrane breakwaters based on potential flow theory, developing analytical solutions and discussing wave reflection/transmission coefficients and membrane deformation. ZHAO et al. [20] employed a CIP viscous flow model to simulate wave interactions with fluid-filled membrane breakwaters, analyzing the effects of internal pressure and elastic modulus, and concluded that lower internal pressure conditions yield more significant wave reflection and energy dissipation. GUO et al. [21] experimentally studied the wave attenuation performance of horizontally and vertically placed flexible membrane breakwaters, analyzing parameters such as membrane porosity. LIU et al. [10, 22] combined piezoelectric membranes with flexible membranes to investigate the linear and nonlinear responses of flexible piezoelectric membranes under wave action, discussing control parameters affecting power generation efficiency and wave attenuation, and found that increasing the operating frequency of piezoelectric materials could enhance energy conversion efficiency.

This study derives the dimensionless motion equations for flexible piezoelectric membrane structures and investigates wave-structure interactions using a numerical wave flume. A prediction method for added mass is presented, the critical control parameter range for linear and nonlinear responses is obtained, and the wave attenuation performance is discussed to provide a theoretical basis for the design and engineering application of flexible piezoelectric membrane structures.

2. Mathematical Model

The schematic diagram of the flexible piezoelectric membrane structure, external circuit, and numerical wave flume is shown in [FIGURE:1]. The structure consists of a central piezoelectric layer covered by insulating flexible membranes

on both sides, connected to an external circuit through electrodes at the ends. Installed at the bottom of the wave flume and filled with liquid, the structure divides the flow field into external and internal domains. Since the membrane thickness is typically on the millimeter scale—much smaller than the structural dimensions—it is modeled as an arc segment with center at O_m. Global coordinates (x, z) and local coordinates (r, θ) are established to describe the flow field and membrane motion, respectively. As the application sea area is not specified and this study focuses on mechanism investigation, the incident wave condition in the numerical wave flume is set as a sinusoidal wave.

2.1 Governing Equations for the Flow Field Based on potential flow theory, both the internal and external flow fields satisfy Laplace' s equation:

$$\nabla^2\phi_e = 0, \quad \nabla^2\phi_i = 0$$

where ϕ is the velocity potential, with subscripts e and i denoting external and internal flow fields, respectively.

On the free surface at $z = \eta(x, t)$, the external flow velocity potential ϕ_e satisfies:

$$\frac{\partial\phi_e}{\partial t} + \frac{1}{2}\nabla\phi_e \cdot \nabla\phi_e + g\eta = 0$$

At the bottom boundary, the velocity potentials satisfy:

$$\frac{\partial\phi_e}{\partial z} = 0, \quad \frac{\partial\phi_i}{\partial z} = 0$$

The normal velocity continuity condition at the flexible piezoelectric membrane boundary is:

$$\frac{\partial\phi_e}{\partial n} = \frac{\partial\phi_i}{\partial n} = \frac{\partial\zeta}{\partial t}$$

where ζ is the radial displacement of the membrane from its equilibrium position.

2.2 Governing Equation for the Flexible Piezoelectric Membrane Given the extremely small thickness of the membrane, inertial forces per unit area are negligible compared to pressure differences across the structure. Thus, only the balance between membrane tension and the pressure difference is considered:

$$p_i - p_e = T_m\kappa$$

where p_i and p_e are internal and external pressures, T_m is the membrane tension per unit width, and κ is the membrane curvature.

The pressure-velocity potential relationship satisfies the unsteady Bernoulli equation:

$$p_e + \rho\frac{\partial\phi_e}{\partial t} + \frac{1}{2}\rho\nabla\phi_e \cdot \nabla\phi_e + \rho g z = 0$$

$$p_i + \rho\frac{\partial\phi_i}{\partial t} + \frac{1}{2}\rho\nabla\phi_i \cdot \nabla\phi_i + \rho g z = 0$$

where ρ is water density, T_{m0} is the initial membrane tension under static equilibrium, and r_I is the initial membrane radius.

Substituting these into the pressure difference equation yields:

$$\rho\frac{\partial}{\partial t}(\phi_i - \phi_e) + \frac{1}{2}\rho(\nabla\phi_e \cdot \nabla\phi_e - \nabla\phi_i \cdot \nabla\phi_i) + T_m\kappa = 0$$

The membrane tension T_m can be expressed as:

$$T_m = T_{m0} + (E_p\tau_p\varepsilon - E_p d_{13} E_e \tau_p) + E\tau\varepsilon$$

where E_p is the piezoelectric layer' s elastic modulus, τ_p its thickness, d_{13} the piezoelectric constant, E_e the electric field strength, E the flexible membrane' s elastic modulus, τ its thickness, and ε the membrane strain.

Given the typically low piezoelectric constant, the term containing d_{13} can be neglected:

$$T_m = T_{m0} + E_p\tau_p\varepsilon + E\tau\varepsilon$$

Under small deformation conditions ($\zeta \ll r_I$), the curvature κ in polar coordinates simplifies to:

$$\kappa = \frac{1}{r_I} - \frac{1}{r_I^2}\frac{\partial^2\zeta}{\partial\theta^2}$$

The membrane boundary conditions at the connection points $\theta = \theta_0$ and $\theta = \theta_1$ are:

$$\zeta(\theta_0, t) = 0, \quad \zeta(\theta_1, t) = 0$$

3. Dimensionless Motion Equations for the Flexible Piezoelectric Membrane

To describe the membrane motion and analyze the main control parameters, the governing equations are nondimensionalized using wave period T, water density ρ, and gravitational acceleration g.

The dimensionless radial displacement $\zeta^* = \zeta/(gT^2)$ is expressed as a Fourier series:

$$\zeta^*(\theta, t^*) = \sum_{k=1}^{M} A_k(t^*) \sin\left(\frac{k\pi}{\Delta\theta}(\theta - \theta_0)\right)$$

where $\Delta\theta = \theta_1 - \theta_0$, and M is the number of modes.

For small wave amplitudes, higher-order terms can be neglected. The dimensionless form becomes:

$$\frac{\partial \zeta^*}{\partial t^*} = -\frac{1}{r_I^*}\frac{\partial^2 \zeta^*}{\partial \theta^2} - \frac{T_m^*}{r_I^{*2}}\frac{\partial^2 \zeta^*}{\partial \theta^2}$$

where $\phi^* = \phi/(g^2T^3)$, $t^* = t/T$, $T_0^* = T_{m0}/(\rho g^3 T^4)$, $r_I^* = r_I/(gT^2)$, and $T_m^* = T_m/(\rho g^3 T^4)$.

The dimensionless curvature $\kappa^* = \kappa g T^2$ is:

$$\kappa^* = \frac{1}{r_I^*} - \frac{1}{r_I^{*2}}\frac{\partial^2 \zeta^*}{\partial \theta^2}$$

The dimensionless membrane tension is:

$$T_m^* = T_0^* + E^* \varepsilon'$$

where the dimensionless membrane elastic modulus $E^* = (E_p \tau_p + E\tau)/(\rho g^3 T^4)$.

The dynamic strain ε' can be expressed as:

$$\varepsilon' = \frac{1}{2r_I^{*2}}\left(\frac{\partial \zeta^*}{\partial \theta}\right)^2$$

Substituting the series expansions and applying orthogonality yields the dimensionless vibration equation for the n-th modal amplitude:

$$\frac{d^2 A_n}{dt^{*2}} + \mu\frac{dA_n}{dt^*} + K_A A_n + K_B A_n^3 = F_{ex,n} + F_{c,n}$$

where:

$$K_A = \frac{n^2\pi^2}{r_I^{*2}\Delta\theta^2}\left(T_0^* + \frac{n^2\pi^2}{\Delta\theta^2}\right)$$

$$K_B = \frac{E^*\pi^4}{4r_I^{*4}\Delta\theta^4}n^2(n^2-1)^2$$

$$M_a = -\int_0^{\Delta\theta}\left[\frac{\partial\Phi_i^*}{\partial t^*} - \frac{\partial\Phi_e^*}{\partial t^*}\right]\sin\left(\frac{n\pi}{\Delta\theta}\theta'\right)d\theta'$$

$$\mu = -\int_0^{\Delta\theta}\frac{\partial}{\partial t^*}(\Phi_i^* - \Phi_e^*)\sin\left(\frac{n\pi}{\Delta\theta}\theta'\right)d\theta'$$

Here, K_A and K_B are dimensionless structural stiffnesses, M_a is dimensionless added mass, μ is the damping coefficient, $F_{ex,n}$ is external excitation, and $F_{c,n}$ is coupling excitation for the n-th mode. Numerical solution methods for this system can be found in LIU et al. [17, 22].

---

4. Analysis and Discussion

4.1 Linear Strain Response of the Flexible Piezoelectric Membrane Equation (22) shows that the membrane response satisfies a nonlinear differential vibration equation with nonlinear coefficient K_B, which is controlled by the dimensionless elastic modulus E^*. When E^* is very small, the nonlinear term can be neglected, reducing the equation to a linear vibration equation and resulting in purely linear response. When E^* exceeds a critical value, the nonlinear term becomes significant, leading to nonlinear response.

For $E^* = 0.0001$, the nonlinear term in Equation (22) is considered negligible, and the membrane exhibits linear response, as confirmed by the dynamic strain time histories shown in [FIGURE:2]. With initial tension $T_0 = 70$ N/m, the strain responses under various wave periods follow sinusoidal patterns, indicating linear behavior. The strain amplitude first increases then decreases with wave period, reaching its maximum at $T = 0.88$ s. Similar linear strain responses are observed for initial tensions ranging from 30 to 100 N/m. For any given initial tension, a period scan always reveals a particular incident wave period that maximizes the strain response.

From Equation (17), the dynamic strain can be expressed as a sum of modal amplitudes. According to LIU et al. [17], the first vibration mode cannot exist independently; its amplitude A_1 is a function of subsequent modal amplitudes A_k ($k \geq 2$). [FIGURE:3] shows the time series of modal amplitudes 2 through 5. Contributions from modes above the fourth are negligible. For $E^* = 0.0001$,

the second and third modes dominate the strain response, with the third mode contributing most significantly. In contrast, LIU et al. [10] found that for E^* values between 0.01 and 0.4, the second mode contributes most to the strain response.

4.2 Natural Frequency of the Flexible Piezoelectric Membrane By varying the incident wave period under different initial tension conditions, the variation of wave transmission coefficient with wave period is obtained, as shown in [FIGURE:4]. For a given initial tension, the transmission coefficient generally first increases, then decreases to a minimum, and subsequently increases again. With $T_0 = 70$ N/m, the transmission coefficient reaches its minimum at $T = 0.88$ s, coinciding with the maximum dynamic strain from [FIGURE:2], indicating resonant response. Resonant behavior is critical for structural design and practical applications. Under linear assumptions, this wave period corresponds to the natural frequency of the membrane structure.

presents the resonant periods under various initial tensions. The resonant period decreases as initial tension increases.

Table 1. Resonant Period of Flexible Piezoelectric Membrane Structure Under Different Initial Tension Conditions

T_0 (N · m^{-1})	Resonant Period T (s)
1.31×10^{-5}	2.43×10^{-5}
4.50×10^{-5}	7.83×10^{-5}
1.24×10^{-4}	2.08×10^{-4}
3.98×10^{-4}	6.33×10^{-4}

4.3 Added Mass of the Flexible Piezoelectric Membrane In the response control equation (22), structural stiffness K_A is primarily determined by dimensionless parameter T_0^*, while K_B is determined by E^*. The added mass depends on velocity potentials of both internal and external flows and cannot be calculated directly. However, neglecting nonlinear stiffness effects allows added mass calculation via linear theory.

From linear vibration theory, the dimensionless resonant frequency $\omega^* = \omega T$ can be expressed as:

$$\omega^* = \sqrt{\frac{K_A}{M_a}}$$

where K_A is dimensionless structural stiffness and M_a is dimensionless added mass.

Using the T_0^* values from resonant conditions in , K_A can be calculated from Equation (23) with $\Delta\theta = 0.64674$, $r_I^* = r_I/(gT^2)$, $r_I = 0.35$ m, T taken as the

resonant period, and $n = 2$. The dimensionless added mass M_a can then be back-calculated using Equation (26).

Dimensional analysis shows that M_a can be expressed as a function of the width-to-wavelength ratio B/L, where B is membrane width (0.6 m in the examples) and L is incident wavelength determined by the dispersion relation:

$$\omega^2 = gk\tanh(kh), \quad L = \frac{2\pi}{k}$$

with water depth $h = 0.3$ m.

[FIGURE:5] shows the variation of M_a with B/L, following a logarithmic relationship:

$$M_a = 0.0131 \ln\left(\frac{B}{L}\right) + 0.0219$$

Knowing the natural frequency allows prediction of M_a, and vice versa, providing theoretical support for structural design.

4.4 Control of Linear and Nonlinear Response The dimensionless elastic modulus E^* is the primary control parameter determining linear versus nonlinear response. A critical E^* value exists: below it, the structure exhibits linear response; above it, nonlinear response emerges. By fixing T_0^* (and thus linear stiffness K_A) and scanning E^*, the critical value can be identified through dynamic response analysis.

For the T_0^* values in , parameter scans were performed across different E^* values.

shows dynamic strain time series for $T_0^* = 1.31 \times 10^{-5}$ with E^* varying from 0.0005 to 0.5. As E^* increases, the strain response gradually deviates from sinusoidal form. For $E^* \leq 0.003$, the response remains linear; for $E^* > 0.003$, nonlinear behavior appears. Thus, $E^* = 0.003$ is identified as the critical value. [FIGURE:7] delineates the control parameter ranges for linear and nonlinear response, with the left side of the curve representing the linear region and the right side the nonlinear region.

4.5 Wave Attenuation Performance [FIGURE:8] shows the variation of transmission coefficient C_T with E^*. For T_0^* ranging from 1.31×10^{-5} to 1.24×10^{-4} (corresponding to wave periods less than 1 s), C_T first increases gradually, then drops sharply, and subsequently increases again with E^*. For T_0^* from 2.08×10^{-4} to 6.30×10^{-4} (periods greater than 1 s), C_T increases monotonically with E^*. At $T_0^* = 1.31 \times 10^{-5}$ and $E^* = 0.01$, the transmission coefficient approaches 0.1. As shown in

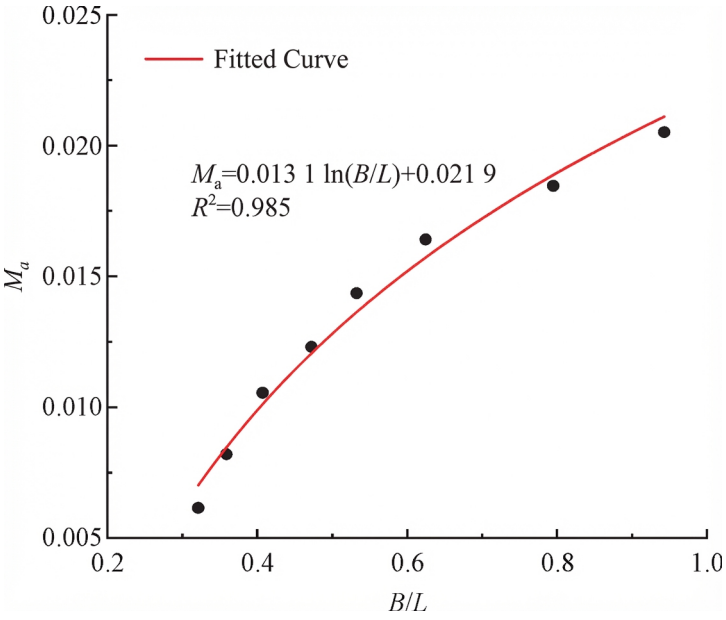

Figure 1: Figure 6

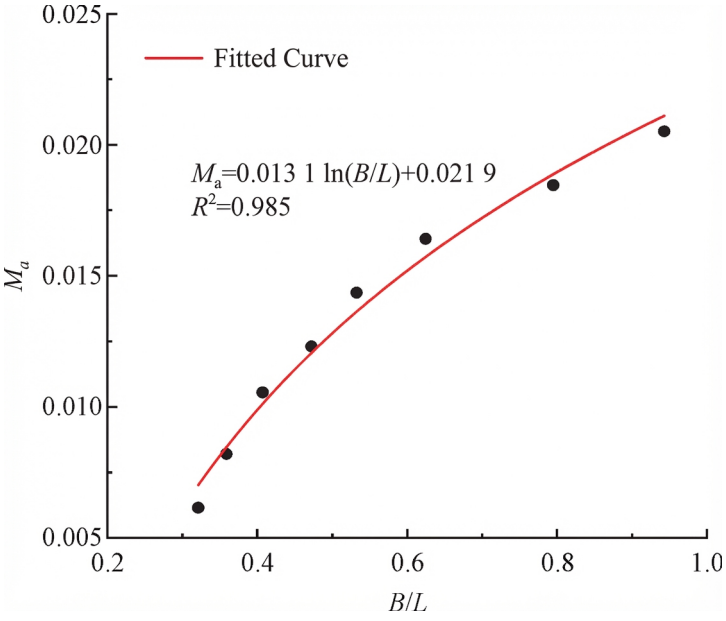

Figure 2: Figure 6

, the membrane response is nearly linear under these conditions. Considering $C_T \leq 0.1$ as indicating excellent wave attenuation, appropriate parameter ranges can be identified: $E^* \leq 0.01$ and $T_0^* \geq 7.83 \times 10^{-5}$.

For design purposes emphasizing wave attenuation, these parameter ranges yield low transmission coefficients. For applications prioritizing energy conversion or balancing both functions, alternative parameter ranges require separate consideration.

---

5. Conclusions

This study derives dimensionless motion equations for flexible piezoelectric membrane structures, identifies primary control parameters, and investigates resonant periods and added mass based on linear assumptions. The critical parameter range for linear response and wave attenuation performance are discussed. Main conclusions are:

1. The dynamic response of flexible piezoelectric membranes under wave action satisfies a nonlinear vibration differential equation controlled by dimensionless elastic modulus E^*. The resonant period is obtained, decreasing with increasing initial tension.
2. The dimensionless added mass M_a follows a logarithmic relationship with B/L, increasing with the ratio. This provides a theoretical basis for predicting added mass and natural frequency.
3. For T_0^* ranging from 1.31×10^{-5} to 6.33×10^{-4}, the critical E^* values distinguishing linear and nonlinear responses are identified, providing theoretical guidance for structural design.
4. Parameter ranges for effective wave attenuation ($C_T \leq 0.1$) are determined as $E^* \leq 0.01$ and $T_0^* \geq 7.83 \times 10^{-5}$.

References

[1] LU Qing, SHI Hongda. Progress and future trend of wave energy technology in China[J]. Coastal engineering, 2022, 41(1): 1-12 (in Chinese).

[2] LIU Yanjun, JIA Rui, ZHANG Jian. Research status and prospect of the wave power generation technology[J]. Journal of ocean technology, 2016, 35(5): 100-104 (in Chinese).

[3] KIRAN M R, FARROK O, ABDULLAH-AL-MAMUN M, et al. Progress in piezoelectric material based oceanic wave energy conversion technology[J]. IEEE access, 2020, 8: 146428-146449.

[4] BURNS J R. Ocean wave energy conversion using piezoelectric material members: EP0274528A1 [P]. 1988.

[5] ZHANG Yongliang, LIN Zheng. Advances in ocean wave energy converters using piezoelectric materials[J]. Journal of hydroelectric engineering, 2011, 30(5): 145-148 (in Chinese).

[6] WU N, WANG Q, XIE X D. Ocean wave energy harvesting with a piezoelectric coupled buoy structure[J]. Applied ocean research, 2015, 50: 110-118.

[7] VIET N V, XIE X D, LIEW K M, et al. Energy harvesting from ocean waves by a floating energy harvester[J]. Energy, 2016, 112: 1215-1222.

[8] NABAVI S F, FARSHIDIANFAR A, AFSHARFARD A. Novel piezoelectric-based ocean wave energy harvesting from offshore buoys[J]. Applied ocean research, 2018, 76: 174-183.

[9] MUTSUDA H, TANAKA Y, DOI Y, et al. Application of a flexible device coating with piezoelectric paint for harvesting wave energy[J]. Ocean engineering, 2019, 172: 170-182.

[10] LIU C R, YANG W Y. Numerical study on the linear and nonlinear behavior of a fluid-filled piezoelectric membrane under gravity waves[J]. China ocean engineering, 2023, 37(5): 768-780.

[11] OHYAMA T, TANAKA M, KIYOKAWA T, et al. Transmission and reflection characteristics of waves over a submerged flexible mound[J]. Coastal engineering in Japan, 1989, 32(1): 53-68.

[12] PHADKE A C, CHEUNG K F. Response of bottom-mounted fluid-filled membrane in gravity waves[J]. Journal of waterway, port, coastal, and ocean engineering, 1999, 125(6): 294-303.

[13] PHADKE A C, CHEUNG K F. Resonance and response of fluid-filled membrane in gravity waves[J]. Applied ocean research, 2001, 23(1): 15-28.

[14] PHADKE A C, CHEUNG K F. Nonlinear response of fluid-filled membrane in gravity waves[J]. Journal of engineering mechanics, 2003, 129(7): 739-750.

[15] STAMOS D G, HAJJ M R, TELIONIS D P. Performance of hemicylindrical and rectangular submerged breakwaters[J]. Ocean engineering, 2003, 30(6): 813-828.

[16] DAS S, CHEUNG K F. Coupled boundary element and finite element model for fluid-filled membrane in gravity waves[J]. Engineering analysis with boundary elements, 2009, 33(6): 802-814.

[17] LIU C R, HUANG Z H. A mixed Eulerian-Lagrangian simulation of nonlinear wave interaction with a fluid-filled membrane breakwater[J]. Ocean engineering, 2019, 178: 423-434.

[18] ZHAO Xizeng, ZHOU Yuwei, YANG Zhijian, et al. Numerical and experimental study on submerged semi-cylindrical membrane breakwater[J]. Shipbuilding of China, 2020, 61(S2): 179-185 (in Chinese).

[19] LI A J, LIU Y, LI H J, et al. Analysis of water wave interaction with a submerged fluid-filled semi-circular membrane breakwater[J]. Ocean engineering, 2020, 197: 106901.

[20] ZHAO X Z, ZHOU Y W, ZONG Y Y, et al. A CIP-based numerical simulation of wave interaction with a fluid-filled membrane submerged breakwater[J]. Ocean engineering, 2022, 260: 111819.

[21] GUO Y C, MOHAPATRA S C, GUEDES SOARES C. An experimental study on the performance of combined membrane breakwaters against incident waves[J]. Ocean engineering, 2023, 280: 114544.

[22] LIU C R, YANG W Y. Theoretical analysis and numerical study on a flexible piezoelectric wave energy converter[J]. International journal of hydromechatronics, 2022, 5(4): 292-310.